Nuclear Instruments and Methods in Physics Research 227 (1984) 267–276
North-Holland, Amsterdam

CATHODE CHARGE DISTRIBUTIONS IN MULTIWIRE CHAMBERS
I. Measurement and theory

J.S. GORDON and E. MATHIESON

Department of Physics, Leicester University, Leicester LE1 7RH, England

Received 23 January 1984 and in revised form 3 April 1984

Detailed measurements under carefully defined conditions have been made of cathode charge distributions in a multiwire chamber Wire and continuous cathodes have been employed These measurements are in close agreement with theoretical predictions which take into account avalanche angular position and spread, and induced charge time development and signal processing

1. Introduction

In order to predict differential non-linearity in position-sensitive multiwire chambers, knowledge of cathode induced charge distributions is required Several groups have, in this connection, described general features of such distributions [1–6] and theoretical accounts have also been given [1,4,7–11]. However, detailed comparisons between measurements and theoretical predictions do not appear to have been made This is understandable since several factors, some of which are difficult to control, affect significantly the experimental distributions These factors are the various chamber geometrical parameters, the angular position and angular spread of the avalanche at the anode wire, positive ion mobility and signal processing time constants.

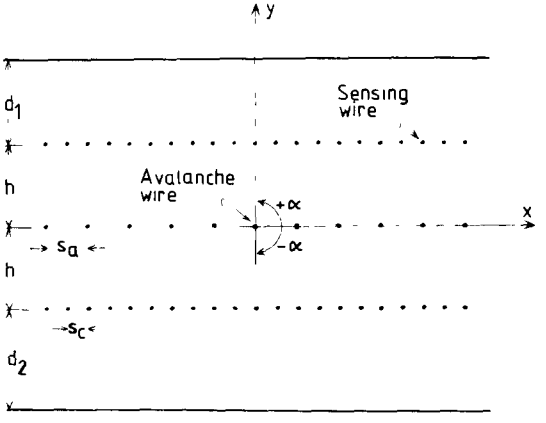

Fig 1 Chamber geometry Anode and cathode wires and the grounded conducting planes are perpendicular to the x, y plane with the avalanche wire at the origin α is the angular position with respect to the x-axis of the avalanche centroid Cathode charge distribution is sampled by an isolated cathode wire.

In most of the present work, in order to define physical conditions as precisely as possible, constant pitch wire cathodes have been employed. Further, the avalanche angular position has been limited to $+\pi/2$ or $-\pi/2$ (see fig. 1 and text below). Experimental results are compared with the predictions of a theoretical model, an extension of an earlier treatment [8], in which account is taken of the finite depth drift spaces behind the wire cathodes. The theoretical treatments of wire and continuous cathodes, given below, have a common basis so that experimental examination of one model may justifiably be regarded as equally examining the other In fact measurements of distributions on a continuous cathode have also been made and are compared with theory below. These measurements, however, presented more experimental difficulties than those with wire cathodes.

2. Theory

2.1. General comments

An important feature of the present theoretical calculations is that prediction is made of the actual distribution that results directly from experimental measurements; signal processing which converts an induced charge waveform into an output voltage peak height is taken into account. Induced charge is calculated by means of the reciprocity theorem [12] a form of which may be briefly stated as follows: if a conductor raised to unit potential produces at an external point a potential P then unit charge placed at that point will induce on the (grounded) conductor a charge $-P$.

The chamber geometry for the present work is shown in fig. 1, all wires are perpendicular to the x, y plane with the avalanche anode wire at the origin Equal

anode/cathode spacings are indicated, and were used, but this is not essential to the theory. The charge development with time on any single wire, or group of wires, is calculated for a 'fan' of several ion trajectories, the initial angular centroid of the fan being at an angle α to the x-axis and the charge for each trajectory being weighted to simulate a Gaussian initial angular spread of avalanche charge with rms value σ The sections below outline the method of predicting the charge $q(t, \lambda, \alpha)$ induced on a single cathode wire at time t and wire position $\lambda = x'/h$. This (numerical) waveform is then convoluted with the processing channel impulse response $h(t)$ to yield the output waveform and hence pulse height $v(\lambda, \alpha)$. In order to remove dependence upon avalanche magnitude, the anode waveform $q_a(t, \alpha)$ is calculated, by essentially the same method, and therefore, after identical signal processing, the anode channel output pulse height $v_a(\alpha)$ is obtained The ratio v/v_a is independent of avalanche charge

It is interesting to compare the wire cathode distribution with that for a continuous cathode, where the function $\rho(\lambda)d\lambda$ represents the charge induced on a strip of width $d\lambda$ at position λ. The wire cathode distribution may therefore be suitably normalised by dividing the single-wire pulse height $v(\lambda, \alpha)$ by the normalised cathode wire pitch s_c/h Hence the distribution function which is predicted by the theory and which can be compared directly with experimental measurement is given by

$$\Gamma(\lambda, \alpha) = \frac{v(\lambda, \alpha) h/s_c}{v_a(\alpha)}.$$

For the continuous cathode, the waveform $\rho(t, \lambda, \alpha)$, calculated by the method outlined below, is convoluted with the impulse response $h(t)$ to yield an output pulse height $v_c(\lambda, \alpha)$ Then *

$$\Gamma(\lambda, \alpha) = \frac{v_c(\lambda, \alpha)}{v_a(\alpha)}.$$

Of the many parameters that enter into the calculation of Γ, all but one may be closely defined by the conditions of measurement The one 'adjustable' parameter in the theory is the avalanche rms angular spread σ

2 2 *Induced charge; wire cathode and anode*

Consider two asymmetrically spaced conducting planes at $y = h + d_1$, and $y = -(h + d_2)$, fig 1, with all anode and cathode wires removed. The potential $P_0(x, y)$ due to uniform line charge of density q_0 perpendicular to the x, y plane, at position x_0, y_0 is given by

$$P_0 = -\frac{q_0}{2\pi\epsilon_0} L(x, x_0, y, y_0), \tag{1}$$

where

$$L = \ln\left[\frac{\cosh a(x - x_0) - \cos a(y - y_0)}{\cosh a(x - x_0) + \cos a(y + y_0 - d)}\right]^{1/2},$$

and

$$a = \pi/2l, \quad l = h + (d_1 + d_2)/2, \quad d = d_1 - d_2$$

Thus replacing the anode and cathode wires by uniform line charges, and assuming $r_a \ll s_a$ and $r_c \ll s_c$, the potential function can be written in general

$$P = -\Sigma C_i L_i, \tag{2}$$

where

$$L_i = L(x, x_i, y, y_i)$$

The summation is taken over all wires in the system, and x_i, y_i is the position of the ith wire. The coefficients C_i can be determined knowing the potentials P_j at the wire surfaces That is

$$P_j = -\Sigma C_i L_{ij}, \tag{3}$$

where

$$\begin{aligned}
L_{ij} &= L(x_j, x_i, y_j, y_i), && i \neq j,\\
L_{jj} &= \ln\frac{ar_c}{2\cos a(h - d/2)}, && \text{for top cathode,}\\
&= \ln\frac{ar_a}{2\cos a\alpha/2}, && \text{for anode,}\\
&= \ln\frac{ar_c}{2\cos a(h + d/2)}, && \text{for bottom cathode.}
\end{aligned}$$

If $P_k = 1$ and all other $P_j = 0$ in eq. (3) then, after solving for the vector C_i, by (numerical) matrix inversion, eq (2) yields $P(x, y)$ the potential due to the kth wire at unit potential, all other wires and surfaces being grounded. From the reciprocity theorem, therefore, the charge induced on the kth wire by unit point charge at x, y is simply $-P(x, y)$

The same method may be used to calculate the induced charge on any group of wires, in particular, on the anode wires. For this case the net charge includes of course both the induced charge and the collected electron charge.

2.3 *Induced charge; continuous cathode*

Suppose, in fig. 1, that the wire cathodes are replaced by continuous conducting cathodes and that, initially, the anode wires are removed. Then if a narrow strip of the top cathode, of width dx' at position x', is held at unit potential, the remainder of that cathode and the other being grounded, the potential $dP_s(x, y)$ between

* In an accompanying paper [13] cathode distributions measured parallel to and orthogonal to the anode wire direction are distinguished by the subscripts 1 and 2 respectively The present paper is concerned with the second case only but, for simplicity, the subscript 2 will not be employed

the cathode planes is given by

$$dP_c = \frac{1}{4}\frac{\cos ay}{\cosh a(x - h\lambda) - \sin ay}\, d\lambda, \quad (4)$$

where $a = \pi/2h$ and $\lambda = x'/h$

Replacing the anode wires (at zero potential) by uniform line charges, of density $2\pi\epsilon_0 dC_i$, the total potential function $dP(x, y)$ becomes

$$dP = dP_c + dP_w, \quad (5)$$

where

$$dP_w = -\Sigma dC_i L_i$$

L_i has been defined in eqs (1) and (2) but in this case $d_1 = d_2 = 0$ Since the anode wire surfaces are at zero potential it must follow that for each wire

$$\frac{dP_c(x_j, y_j)}{d\lambda} = \Sigma \frac{dC_i}{d\lambda} L_{ij}$$

The vector $dC_i/d\lambda$ may be found by numerical inversion of this set of equations and hence the potential function $dP/d\lambda$ obtained from eq (5) Then from the reciprocity theorem the charge $\rho(\lambda)d\lambda$ induced on the cathode strip $d\lambda$ by unit point charge at x, y is just $-dP$ That is

$$\rho(\lambda) = -dP/d\lambda.$$

2 4 *Time development of induced charge*

In order to follow the time development of induced charge it is necessary to construct the ion trajectory $x(t), y(t)$. Let the operating anode and cathode potentials be V_a and V_c respectively Then if the vector C_i is found by numerical inversion of eq. (3) with $P_j = 1$ for all anode wires and $P_j = V_c/V_a$ for all cathode wires, the potential function in the operating system is simply $V_a P(x, y)$, where $P(x, y)$ is given by eq. (2). The field components E_x, E_y are obtained by partial differentiation of eq. (2), and the increments in position dx, dy in a small time interval dt are given by $\mu E_x dt$, $\mu E_y dt$ where μ is the positive ion mobility (assumed constant, see section 4.1) Thus

$$\frac{dx}{s_a} = \frac{dt}{T_0}\Sigma C_i \frac{\partial L_i}{\partial x} s_a, \quad \frac{dy}{s_a} = \frac{dt}{T_0}\Sigma C_i \frac{\partial L_i}{\partial y} s_a,$$

where $T_0 = s_a^2/\mu V_a$, a convenient dimensional constant in many wire chamber calculations (of the order 7 μs in the present work).

By starting at $x = r_a \cos \alpha_m$, $y = r_a \sin \alpha_m$ at $t = 0$ and incrementing in sufficiently small intervals dt/T_0, the ion path $x(t), y(t)$ can be constructed and therefore at each stage the induced charge on any wire or group of wires For the continuous cathode calculation of course we have $d_1 = d_1 = 0$ in eq. (2), and $V_c = 0$.

In the complete calculations the total induced charge $q(t)$ on an electrode is found as the sum of the induced charges due to a fan of N ion trajectories, each weighted in charge to represent an initial gaussian angular distribution of avalanche charge The total angular width of the fan was normally taken as 2fwhm = 4 710σ where σ is the rms angular spread. That is

$$q(t) = -\Sigma w_m P(x, y),$$

where

$$w_m = \tfrac{1}{2}\{\mathrm{erf}(u_2) - \mathrm{erf}(u_1)\},$$

and

$$u_{2,1} = \frac{4\,710}{\sqrt{2}}\frac{m \pm 1/2}{N},$$

$$m = -(N-1)/2, \ldots, +(N-1)/2.$$

The initial angle of the mth trajectory is $\alpha_m = \alpha + 4\,710 m\sigma/N$ where α is the avalanche angular centroid For the present signal processing time constants it was found that $N = 5$ was a sufficiently dense representation. For the determination of single cathode wire charge waveforms at times comparable with ion collection times it is of course necessary to employ considerably larger values of N

2.5 *Signal processing*

Channel output voltage $v(t)$ is found from an electrode charge $q(t)$ by convolution with the impulse response $h(t)$ That is

$$v(t) = \frac{1}{C_F}\int_0^t q(t')h(t - t')dt',$$

where C_F is the channel conversion gain (assumed the same for both cathode and anode channels). The actual forms employed for $h(t)$ are given in the appendix.

2 6. *General predictions*

Although detailed, quantitative comparisons between prediction and measurement are given later, it is convenient to note briefly here some important general features. Fig. 2 demonstrates that the angular position of the avalanche is indeed a sensitive parameter in determining the distribution. The same figure also demonstrates that wire and continuous cathode distributions may differ quite significantly

The ratio of the maxima of the distributions for $\alpha = +\pi/2$ and $\alpha = -\pi/2$ is found, as to be expected, strongly dependent on the signal processing time constant This is shown quantitatively in fig. 3, for the extreme case $\sigma = 0$

A further, important general prediction of the calculations is that the distributions for $\alpha = +\pi/2$ and $-\pi/2$ may differ significantly in shape as well as in magnitude This is illustrated in fig. 4 where the two distribu-

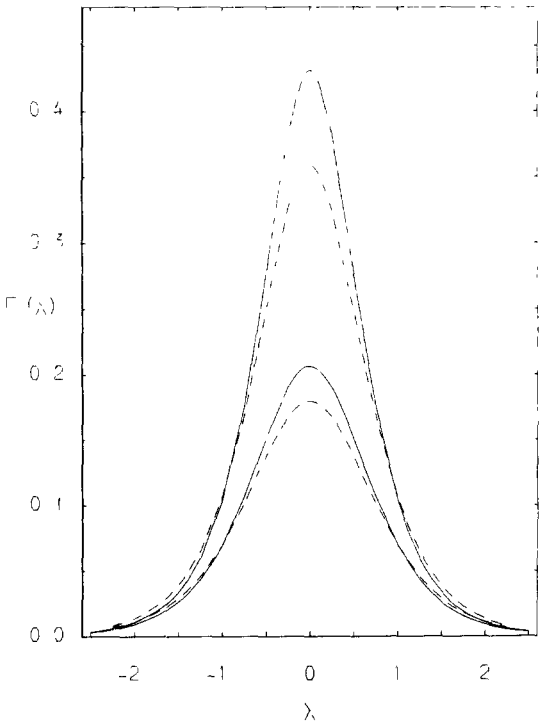

Fig. 2 Cathode distribution function $\Gamma(\lambda)$. Theoretical predictions for $\alpha = +\pi/2$ and $-\pi/2$ for continuous cathodes (upper and lower continuous curves respectively) and for wire cathodes (upper and lower broken curves) The predictions are for 'standard conditions' (see section 4.1)

tions have been normalised to equal area. This shape difference may have important practical effects in position encoding under certain conditions.

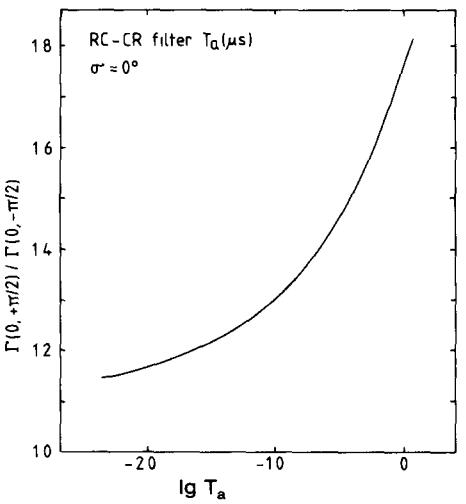

Fig 3 Predicted ratio of maxima of cathode distribution functions for $\alpha = +\pi/2$ and $-\pi/2$. Standard conditions, but with avalanche spread $\sigma = 0°$ and with CR–RC filter.

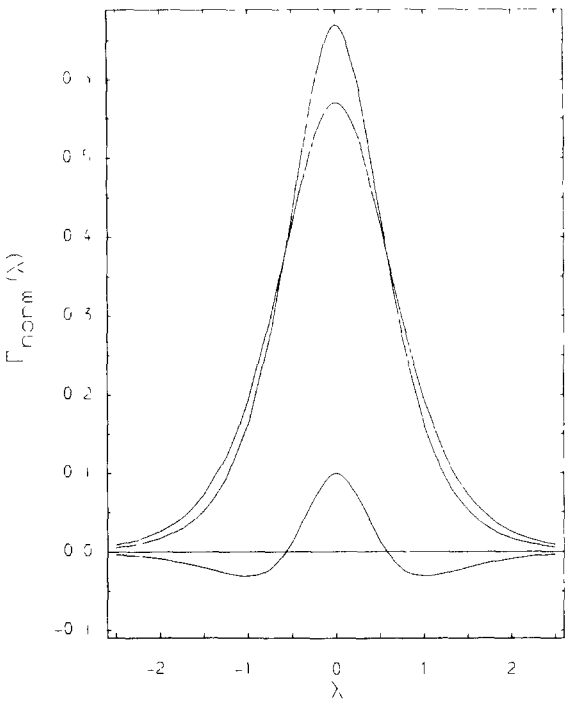

Fig 4 Predicted cathode distribution functions, for $\alpha = +\pi/2$ and $-\pi/2$, standard conditions but with continuous cathodes, normalised to equal area (unity) This figure illustrates the difference in shape between the two distributions The bottom curve is the difference $\Gamma_{no}r_m(\lambda, +\pi/2) - \Gamma_{norm}(\lambda, -\pi/2)$

3. Experimental method

The essential requirements of the experimental apparatus were that physical conditions be defined as precisely as possible, and that relevant parameters could be adjusted within typical ranges These requirements were facilitated by the use of a small, flexible chamber with a flow gas system, and standard electronic units. Fig. 5 illustrates the overall arrangement schematically

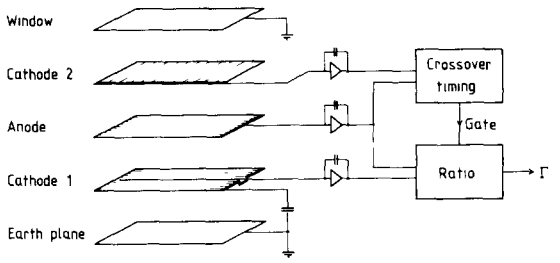

Fig 5 Schematic diagram of experimental arrangement The isolated sampling wire is contained in cathode 1 The signal from cathode 2 is employed to differentiate between $\alpha = +\pi/2$ and $\alpha = -\pi/2$ events

A conducting aluminium foil plane and the detector entrance window defined the two drift spaces, with adjustable depths d_1 and d_2 respectively (referring also to fig 1). 100×100 mm^2 wire arrays with various constant wire pitches (s_a and s_c for anode and cathodes respectively) and radii (r_a and r_c) could be utilised at selectable anode–cathode spacing (h), with the wires aligned orthogonal or parallel. All important geometrical parameters were the subject of careful measurement

The wire cathode on which the distribution of induced charge was to be measured had one wire at the centre isolated from the remainder (but maintained at the same potential) and connected to a signal processing channel identical, except for a wide band attenuator, to that of the anode Output signal pulse heights were digitised, and the ratio of single cathode wire pulse height to anode pulse height displayed The attenutator allowed the working ratio to be kept to the order unity, and a careful measurement of the relative conversion gains of the two channels allowed true ratios to be calculated.

Particular care had to be taken to ensure negligible charge induction on the single cathode wire by voltage excursions of other chamber electrodes The remaining wires of cathode 1 were connected to earth through a capacitor ($\sim 1\ \mu$F) very large compared to the interwire capacitance. Pre-amplifiers with large (~ 9000 pF) dynamic input capacity were used.

For measurement of the induced charge distribution on a continuous cathode, a copper-clad G10 board was used as cathode 1, and an aluminium foil (25 μm), transparent to the X-rays, as cathode 2. On cathode 1 a strip of width 0.8 mm, isolated by gaps of 0.2 mm, sampled the induced charge distribution, a high resistivity coating being applied to the gaps to prevent local field distortion The effective sampling width dλ was taken as 1.0 mm

A parameter not generally controlled in an operating MWPC is the avalanche angle centroid, α. The cathode induced charge distribution is a strong function of this parameter however, and α therefore had to be defined for the present measurements It has been shown [14,15] how the crossover time of a doubly differentiated cathode signal varies with α, and is thus a two-valued function of the position of a collimated X-ray beam moving perpendicular to the anode wires Fig. 6 shows typical variation obtained from cathode 2 signals processed with a 1 μs bipolar filter. Anode wire positions may be simply determined as those values of x where the crossover difference is greatest. In the present work, avalanche angle centroids of essentially $+\pi/2$ and $-\pi/2$ were defined by only sampling cathode induced charge distribution for X-ray source positions coincident with anode wire positions When the single cathode wire was sensing the tails of distributions, where the difference between $+\pi/2$ and $-\pi/2$ avalanche centroid events is small, gating derived from the crossover spectrum from cathode 2 allowed selection of one or the other type of event Fig 7 shows a typical crossover spectrum, with the two types of event clearly differentiated Such gating also allows measurement of distributions parallel to the anode wires, when physical limitation of the avalanche angle is not possible, given a slit collimator.

The only important experimental parameter which could not be directly controlled was the rms angular spread, σ, of the avalanche about its centroid Two precautions were taken to limit σ and to keep its value relatively constant Application of a negative potential to the wire cathodes made the counter insensitive to X-rays absorbed in the drift regions, and thus reduced variation in σ arising from differing amounts of electron diffusion. Secondly, the chamber was operated at a charge level such that UV spreading of the avalanche was a minor contribution [16] The degree of avalanche localisation around the wire is reflected in the difference between $+\pi/2$ and $-\pi/2$ induced charge distributions, with the obvious limit that there is no distinction if the

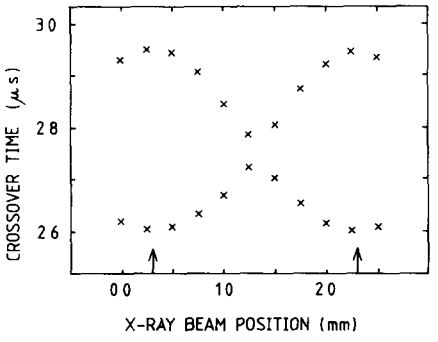

Fig. 6 Cathode 2 signal cross-over time measured as a function of X-ray beam position, x_0 The two values of cross-over time correspond to $+\alpha$ and $-\alpha$ where $\alpha = (1 - 2x_0/s_a)\pi/2$

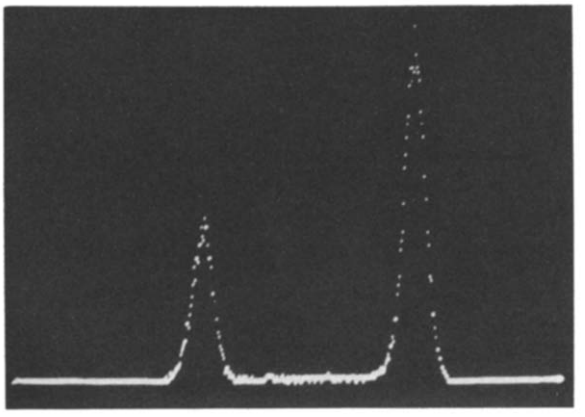

Fig 7. A typical spectrum of cathode 2 signal cross-over times, illustrating the clear differentiation between $\alpha = -\pi/2$ and $\alpha = -\pi/2$ events obtainable with a 1 μs bipolar filter

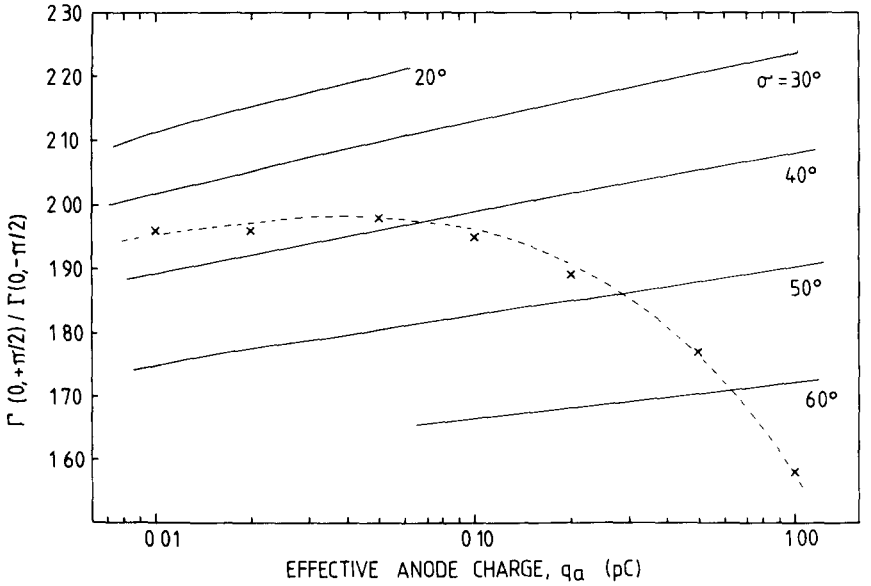

Fig 8 Determination of rms avalanche spread σ Theoretical predictions (continuous curves) and experimental measurements (crosses) of ratio of maxima of cathode distribution for $\alpha = +\pi/2$ and $\alpha = -\pi/2$ All measurements in section 4 were taken at 0 1 pC effective anode charge, corresponding theoretical predictions were made with $\sigma = 40°$

avalanche spreads evenly around the wire. Fig 8 illustrates how the ratio of the heights of the centres of the two distributions, $\Gamma(0, +\pi/2)/\Gamma(0, -\pi/2)$, under standard conditions as defined in section 4.1 below, varies with anode charge level, the effect of rapidly increasing angular spread above about 0.1 pC being apparent. The anode and cathode potentials employed to produce the charge levels shown were used in theoretical calculations of the ratio $\Gamma(0, +\pi/2)/\Gamma(0, -\pi/2)$ with various values of the angular spread to give the continuous lines shown. The results in section 4 were obtained at 0.1 pC anode charge, the corresponding calculations all using the rms value $\sigma = 40°$.

The requirement to work at a relatively low chamber gain demanded a low noise in the single cathode wire channel. An equivalent noise charge of 200 electrons rms at the 2μs time constant was obtained allowing measurement of the induced charge distribution out to $\lambda = 3$ from the centre without undue difficulty. The noise level when the strip on the continuous cathode was connected to the processing channel was an order of magnitude worse, due to the (unoptimised) resistive coating.

4. Results

Some results are presented which test the validity of the predictions of the theoretical model presented in section 2 over a range of parameters. Corresponding $\alpha = +\pi/2$ and $\alpha = -\pi/2$ distributions that were obtained concurrently are presented together, and the relevant predictions are shown as curves rather than discrete points (see section 2). The comparisons are direct, no arbitrary normalisation having been introduced

Stochastic errors, arising from the location of the centroids of $\Gamma(\lambda, +\pi/2)$ and $\Gamma(\lambda, -\pi/2)$ at any λ, and from the measurements of relative channel conversions gains, were smaller than could be shown clearly in the figures The size of the symbols used for the data points may be taken as indicating maximum error boxes

4 1 Standard conditions, and the effect of cathode 2 orientation

The experimental strategy involved defining a set of 'standard' parameters, then observing how the complete distributions were affected by changes to one type of parameter This basic set of conditions was·

i) Chamber geometry (see fig. 1). $h = 4$ mm, $s_a = 2$ mm, $s_c = 1$ mm, $r_a = 7.5$ μm, $r_c = 25$ μm, $d_1 = d_2 = 4$ mm.

ii) Chamber gas. Ar 50% CH_4, positive ion mobility, μ,* taken as 2 0 $cm^2V^{-1}s^{-1}$ [17]

* It is known that μ is field dependent [18] although there exists little relevant data for most counter gases Calculations with a field dependent mobility in the form $\mu = \mu_0/\sqrt{(1+E/E_0)}$ reveal that, with the present time constants and geometry, an experimentally significant effect ($\gtrsim 2\%$) occurs only when E_0 is chosen below about 25 kV/cm In view of the generally good agreement between measurement and prediction this must represent a lower limit for E_0 for P50

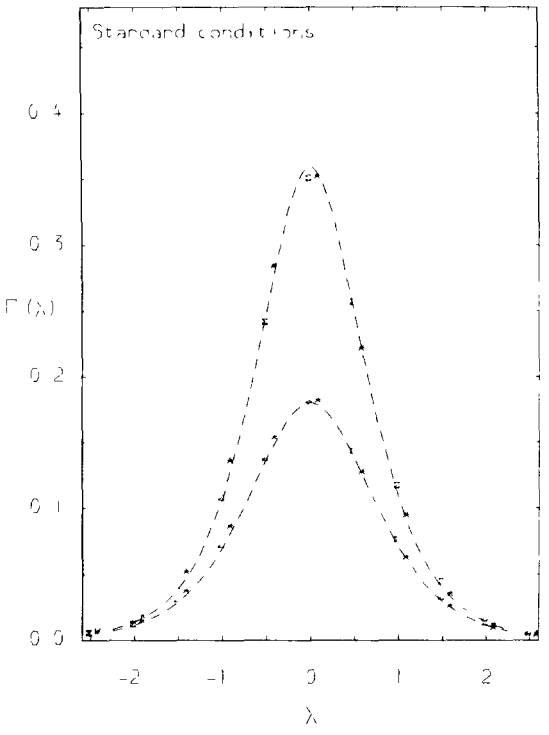

Fig. 9 Cathode distribution functions $\Gamma(\lambda)$ Comparison between experimental measurements and theoretical predictions ($\alpha = +\pi/2$ upper curve, $\alpha = -\pi/2$ lower curve), standard conditions (see section 4 1)

iii) Signal processing. Canberra 2022 'Gaussian' active filter, nominal time constant 2 μs

1 5 keV AL K_α X-rays were used for all measurements. Fig. 9 shows experimental data and theoretical predictions for these standard conditions. The two sets of experimental points were taken with cathode 2 wires parallel to and orthogonal to those of the anode and cathode 1. There is no discernable difference, and all subsequent readings were taken with the two sets of cathode wires orthogonal to each other.

4 2. Time development

Figs. 10a and 10b show the effect of reducing the processing time constant to a nominal 0 5 μs or increasing to 4 μs respectively (see appendix). The expected increasing difference between $\Gamma(\lambda, +\pi/2)$ and $\Gamma(\lambda, -\pi/2)$ as the distributions are effectively sampled later in time may be noted. The significant parameter is the ratio of the chamber time unit $T_0 = s_a^2/\mu V_a$ to the filter effective time constant. Good agreement between prediction and measurement was also obtained when a simple CR–RC filter was used, sampling the distribution earlier than the 2022 filter for the same nominal time constant Similar agreement was observed when Ar

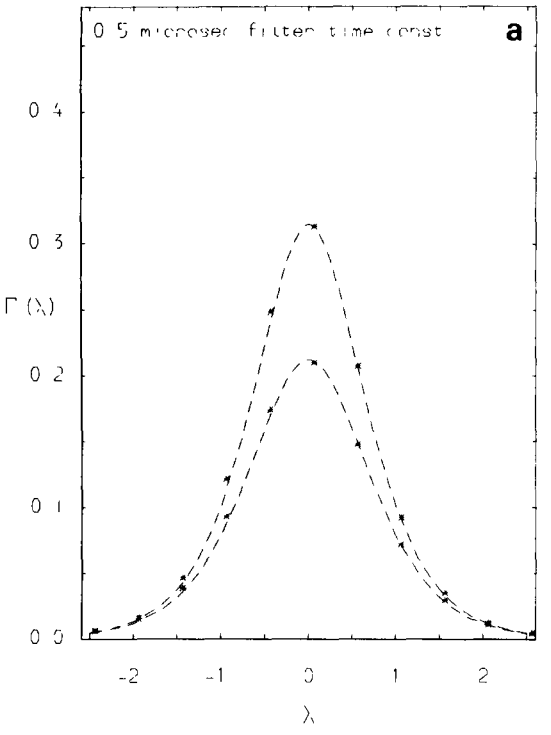

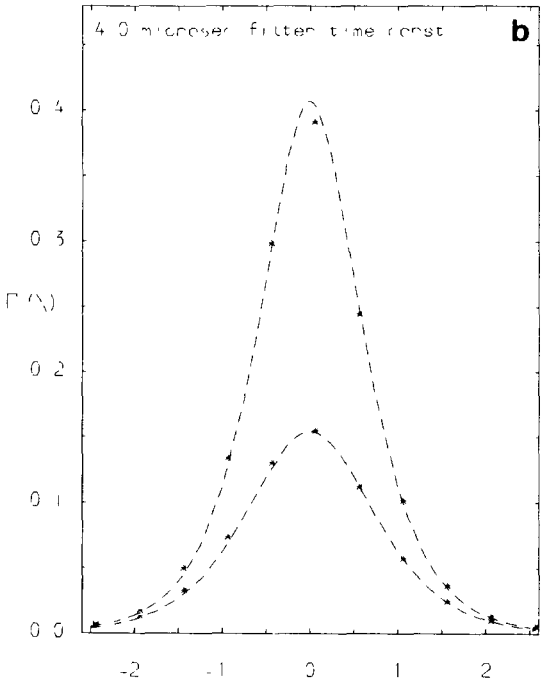

Fig. 10 Cathode distribution function $\Gamma(\lambda)$ Comparison between experimental measurements and theoretical predictions ($\alpha = +\pi/2$ upper curve, $\alpha = -\pi/2$ lower curve), (a) standard conditions except with $T_a = 0\,5$ μs, (b) standard conditions except with $T_a = 4\,0$ μs.

10% CH_4 gas was used, giving a longer chamber time unit T_0 than Ar 50% CH_4 (mainly because of the decrease in V_a for the same charge).

4 3 The influence of earth planes behind wire cathodes

Measurements made with the continuous cathode described in section 3 are shown in fig. 11. The effect of 'charge leakage' to earth planes behind wire cathodes may be clearly seen by comparing with fig. 12, where the data is for the standard parameters except for the use of 2 mm, rather than 1 mm, pitch cathodes

4 4 The effect of anode–cathode spacing

Good agreement was maintained when the anode–cathode spacing was increased to 6 mm (fig 13) Although the distributions are broader at larger h in absolute units, the difference in terms of λ can be seen to be small.

4 5 Distributions parallel to the anode wires

The theoretical curves in fig. 14 are for the standard conditions, the experimental data are for these conditions but with the anode rotated through 90°. While the model predicts specifically the distribution of cathode charge perpendicular to the anode wires, it may be seen that it also provides a reasonably close description of the distribution parallel to the anode wires.

A theoretical study is now being carried out in an attempt to predict cathode distributions in a direction parallel to the anode wires with the same accuracy as the present theoretical distributions.

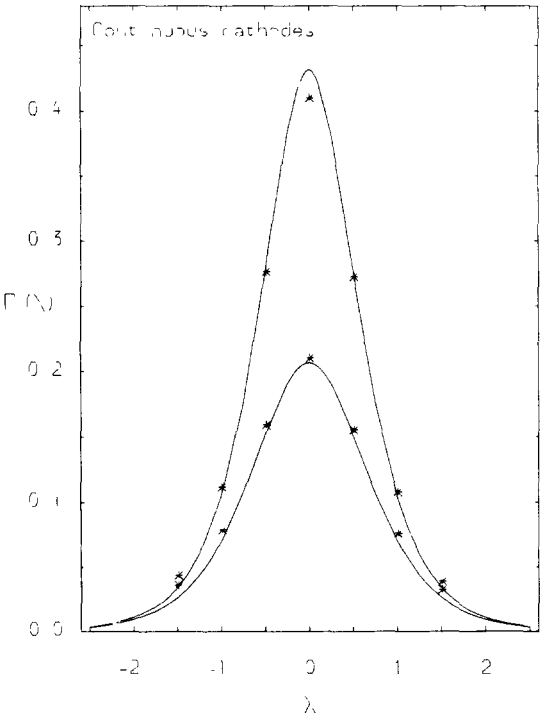

Fig. 11 Cathode distribution functions $\Gamma(\lambda)$ Comparison between experimental measurements and theoretical predictions ($\alpha = +\pi/2$ upper curve, $\alpha = -\pi/2$ lower curve), standard conditions but with continuous cathodes

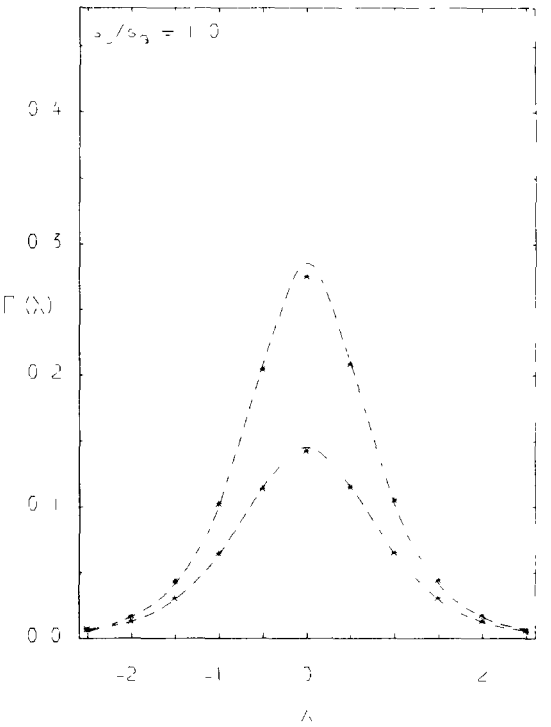

Fig 12 Cathode distribution functions $\Gamma(\lambda)$ Comparison between experimental measurements and theoretical predictions ($\alpha = +\pi/2$ upper curve, $\alpha = -\pi/2$ lower curve), standard conditions except with $s_c = 2$ mm

5. Conclusions

Close agreement has been obtained, over a wide range of conditions, between experimental measurements of cathode induced charge distribution and the predictions of a theoretical model. This agreement has been made possible by, on the one hand, precisely defining experimental conditions (e g., use of wire cathodes) and, on the other, including in the calculations the avalanche angular position and spread and a full treatment of signal time development and processing The model may therefore be used with considerable confidence to calculate, for the geometry of fig. 1 and given appropriate initial conditions, the charge distribu-

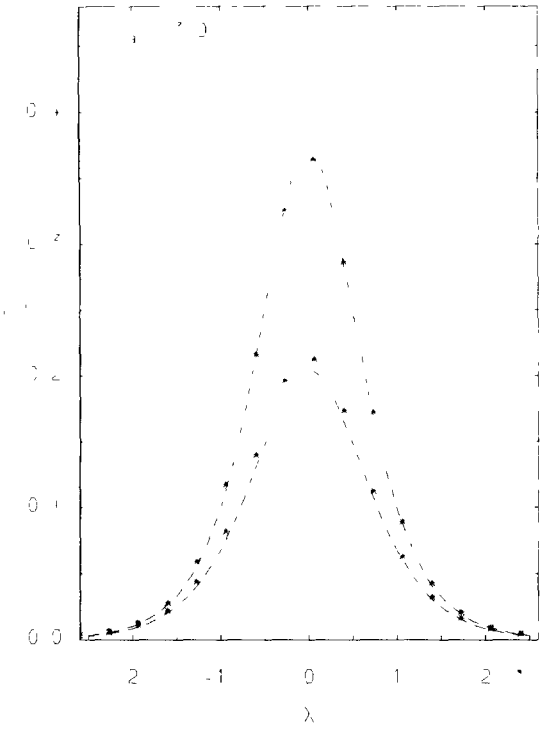

Fig 13 Cathode distribution functions $\Gamma(\lambda)$ Comparison between experimental measurements and theoretical predictions ($\alpha = \pi/2$ upper curve, $\alpha = -\pi/2$ lower curve), standard conditions except with $h = 6$ mm

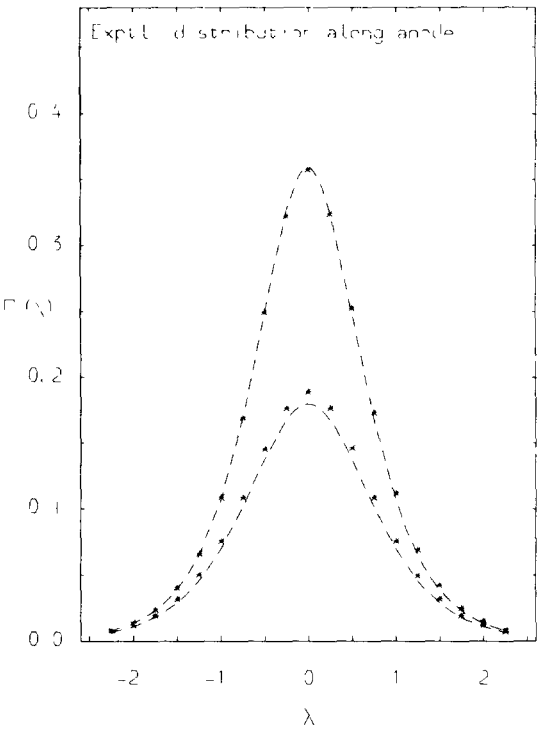

Fig 14 Cathode distribution functions $\Gamma(\lambda)$, measured parallel to the anode wire direction The theoretical predictions are for distributions perpendicular to the anode wire direction

tions on wire or continuous cathodes, or indeed on any group of electrodes, or to calculate output pulse heights from a signal processing channel attached to any group of electrodes

The original motivation for this work, the prediction of differential non-linearities in position-sensitive MWPCs, now however has to be re-assessed. Detailed prediction, such as the above model now makes possible, is not generally required; avalanche angular position is not determined in a practical system In this case a single formula for the cathode distribution, convenient for computation and representing an average behaviour, is required. In an accompanying paper [13] an existing empirical formula [9] is compared with the results of accurate calculations and it is shown that this formula may be presented in a convenient single parameter form over a wide range of practical geometries

We wish to thank Dr G. Smith (now at Brookhaven National Laboratory, USA) for his initial suggestions, and Dr.J Leake (AERE, Harwell, UK) for continued interest and assistance J.S.G. acknowledges financial support from SERC and AERE

Appendix

The present experimental studies employed two types of signal processing. The majority of measurements were made with Canberra type 2022 spectroscopy amplifiers in both channels. For this system (one differentiator, two active integrators) the impulse response is determined by two circuit time constant T_1, T_2 and may be shown to be given by

$$h(t) = \frac{T_2}{(T_2 - T_1)^2}\, e^{-t/T_2}\left\{\left(1 - \frac{w^2 T_2 t}{2}\right)\cos wt + \frac{wT_2}{2}\left(1 + \frac{t}{T_2}\right)\sin wt - 1\right\},$$

where

$$w = (T_2/T_1 - 1)^{1/2}/T_2$$

The nominal time constant T_a employed in the text above corresponds to values of T_1 and T_2 as follow.

T_a (μs)	0.50	2.00	4.00,
T_1 (μs)	0 29	1.15	2.30,
T_2 (μs)	0 43	1.69	3.38.

Measurements were also taken with simpler amplifiers containing equal time constant, single integration, single differentiation signal processing. For this system $h(t)$ is given by

$$h(t) = \frac{1}{T_a} e^{-t/T_a}\left(1 - \frac{t}{T_a}\right).$$

References

[1] G Fischer and J Pich, Nucl. Instr Meth 100 (1972) 515

[2] G Charpak and F. Sauli, Nucl Instr and Meth. 113 (1973) 381

[3] A Breskin, G Charpak, C. Demierre, S Majewski, A Policarpo, F Sauli and J.C Santiard, Nucl Instr and Meth 143 (1977) 29.

[4] I Endo, T Kawamoto, Y. Mizuno, T Ohsugi, T Taniguchi and T Takeshita, Nucl. Instr and Meth 188 (1981) 51

[5] G Piuz, R Roosen and J Timmermans, Nucl Instr and Meth 196 (1982) 451

[6] J Chiba, H Iwasaki, T Kageyama, S Kuribayashi, K Nakamura, T Sumiyoshi and T Takeda, Nucl Instr and Meth 206 (1983) 451

[7] D Lee, S Sobottka and H Thiessen, Nucl Instr and Meth 104 (1972) 179

[8] E Mathieson, Nucl Instr and Meth 159 (1979) 29

[9] E Gatti, A Longoni, H Okuno and P Semenza, Nucl Instr and Meth 163 (1979) 83

[10] G A Erskine, Nucl Instr and Meth 198 (1982) 325

[11] H van der Graaf and J P Wagenaar, Nucl Instr and Meth. 217 (1983) 330

[12] W R Smythe, Static and dynamic electricity (McGraw-Hill, New York, 1968) p 35

[13] E Mathieson and J S Gordon, Nucl Instr and Meth 227 (1984) 277

[14] C J Borkowski and M K Kopp, IEEE Trans Nucl Sci NS-24 (1977) 287

[15] P J Gilvin, E Mathieson and G.C Smith, IEEE Trans Nucl Sci NS-27 (1980) 101

[16] H Okuno, J Fischer, V Radeka and A Walenta, IEEE Trans Nucl Sci NS-26 (1979) 160

[17] G Schultz, G Charpak and F Sauli, Rev. Phys Appl 12 (1977) 67

[18] S C Brown, Basic data of plasma physics (MIT, Cambridge, 1977)